JOURNAL OF PROPULSION AND POWER
Vol. 15, No. 4, July–August 1999

Dynamic Modeling of Hybrid Rocket Combustion

M. Arif Karabeyoglu* and D. Altman†
Stanford University, Stanford, California 94305

The combustion dynamics in hybrid rockets is studied to provide a basic input into transient motor processes. The model treats the time-dependent heat flow into the ablating fuel surface. A variable surface temperature is considered with an effective activation energy to describe the surface-temperature variation during the transient. Two time scales are observed for throttling: a short lag near the surface related to the activation energy, and the larger well-known thermal lag as a result of conductivity. The model is also applied to an oscillating surface heat-flux input. We observed an amplification of the regression-rate oscillations for low frequencies. Although this effect is not the cause of instability, it can aggravate existing oscillations at these low frequencies. We next formulated a quasisteady combustion model, which is then coupled with the thermal lag system with boundary-layer delays that account for the adjustment of the boundary layer to the changes in the freestream conditions and blowing from the surface. A linearized treatment of this coupled system evidences some low-frequency instabilities. The scaling of the oscillation frequencies and the erratic character of the experimentally observed instabilities are successfully explained.

Nomenclature

A	= pre-exponential coefficient
A_p, A_n	= port and nozzle throat areas
B_a, B_t	= aerodynamic and thermochemical blowing parameters
C	= specific heat of fuel
C_f, C_H	= skin-friction coefficient and Stanton number
c'	= boundary-layer delay time coefficient
c^*_{exp}, c^*_{theo}	= measured and calculated characteristic velocities
D	= port diameter
E_a	= activation energy
E_L, E_h, E_{E_a}	= energy parameters, see the Appendix
G_o, G_t	= oxidizer and total mass fluxes
h_v, L_v	= total and latent heats of gasification
I	= Laplace transform of oxidizer mass flux
k	= blowing parameter exponent
L	= length of the fuel port
n	= mass flux exponent
P_c	= chamber pressure
$\dot{Q}_c$, $\dot{Q}_w$	= convective and total wall heat fluxes
R_g	= specific gas constant
$\dot{r}$, R	= dimensional and nondimensional regression rate
s	= Laplace transform variable
u, v	= axial and normal velocities
V_p, V_m	= port and motor volumes
x	= coordinate in the solid fuel
y, z	= coordinate normal to the surface and axial distance along the port
κ	= thermal diffusivity of fuel
λ	= thermal conductivity of fuel
μ	= viscosity
ρ_f	= density of fuel
σ_1, σ_2	= gas phase response coefficients
τ_{b1}, τ_l	= boundary-layer response time and thermal lag time
ω, f	= angular frequency and frequency

Subscripts

b	= flame value
e	= freestream value
f	= fuel
o	= oxidizer
ref	= reference quantities
s	= surface
1	= first perturbation variable

Superscripts

qs	= quasisteady
$-$	= nondimensional variable

Introduction

IN the scaling of hybrid motors to larger sizes, two problem areas that have been identified are 1) motor instability (particularly nonacoustic low-frequency modes) and 2) delayed transients in ignition, throttling, and shutdown. We believe that an understanding of the transient phenomena in the motor is essential to explain the low-frequency pressure oscillations observed in practice. Although the theory for steady-state burning rate has been established for some time,[1–3] the literature treating transient regression rate in hybrids is deficient. This is particularly true in treating the overall motor transient behavior.

For a full description of motor transients, one has to consider response times resulting from 1) feed system dynamics, 2) vaporization of the liquid oxidizer, 3) diffusion processes in the boundary layer, 4) combustion mechanisms in the flame zone, 5) chamber gasdynamics, and 6) thermal profile changes in the solid grain. The order of magnitude estimates of the time scales of some of those processes are discussed in Ref. 4. Our approach is to isolate each of the transient phenomena considered in the previous paragraph and to develop physical/chemical models for those isolated phenomena. In this paper we have limited our investigations to the thermal lags in the solid and to the hybrid boundary-layer combustion dynamics, i.e., the delay between mass flux and heat transfer to the wall. These isolated models for the thermal lags and combustion dynamics will later be coupled to obtain the overall transient response of the hybrid combustion.

Thermal Lags in the Solid

The regression rate of the hybrid fuel grain cannot respond to the changes in the surface heat flux instantaneously because of the

Received 16 April 1998; revision received 12 October 1998; accepted for publication 29 October 1998.

*Doctoral Student, Department of Aeronautics and Astronautics. Student Member AIAA.

†Consultant; currently Senior Vice President, Chemical System Division, United Technology Corporation, 1670 Oak Avenue, Menlo Park, CA 94025 (Retired). Fellow AIAA.

finite thermal conductivity of the solid fuel. This phenomenon was investigated approximately by Marxman et al.,[2] and more recently by the authors.[5] In this paper we further study the throttling event to understand the effect of the activation energy and the throttling rate on the response of the thermal lag system. The thermal lag treatment will then include the response of the regression rate to a sinusoidally varying wall heat flux. The thermal lag model is shown in Fig. 1, and the mathematical formulation and various solution techniques are presented in Ref. 5. However, for the sake of completeness, some important aspects of the theory are summarized in the Appendix.

With use of the techniques presented in Ref. 5, several new simulations of the throttling event are performed to investigate the impact of activation energy and throttling rate. The response of the regression rate for various activation energies to a sudden increase in the surface heat flux for a hydroxyl terminated polybutadiene (HTPB) system is shown in Fig. 2. It can be seen that the activation energy has a significant impact. The common feature is the initial overshooting of regression rate and the relaxation back to the target equilibrium state. However, at high activation energies, E_a, the regression rate overshooting is more pronounced and it reaches its maximum value in a rather short time compared with the thermal relaxation time, t_{t1}. In the other extreme of a very low value of activation energies, the overshooting phenomenon is less significant and is similar to the behavior of a first-order system, where the response approaches the steady-state asymptotically. These observations indicate that the thermal lag system has two time scales, one relating to the initial overshoot and the other to the relaxation. The surface time scale that governs the overshooting is related to the changes in the temperature profile in a small zone next to the wall. The larger time scale is the well-known thermal relaxation, i.e., $\kappa/\dot{r}^2$, which determines the relaxation process from the exited to the equilibrium state.

The effect of activation energy on these time scales is of fundamental importance. The surface time scale depends on the change in surface temperature, which is related to the activation energy through the Arrhenius equation, $\dot{r} = Ae^{-E_a/RT_s}$. Thus, for a given change in $\dot{r}$, the larger the value of E_a, the smaller the change in surface temperature, and consequently, the shorter the time for surface-temperature adjustment. However, the thermal time scale is unaffected by the activation energy, because it is essentially related to the heat-diffusion process in the solid. The effect of these time scales on the transient regression rate can be seen from the energy balance at the surface:

$$\dot{Q}_w = \dot{r}\rho_f L_v - \lambda\left(\frac{\partial T}{\partial x}\right)_s \tag{1}$$

The surface temperature gradient $(\partial T/\partial x)_s$ is negative and adjusts slowly in accordance with the thermal time scale. Thus, at high activation energies for which the surface temperature excursion is short, very little diffusion takes place over the span of the surface time scale. As a result of this, the overshooting is significant. In the opposite extreme of low activation energies, the surface time scale becomes comparable to the thermal time scale and the thermal diffusion makes the overshooting less apparent.

It is instructive to consider the more practical case of the finite throttling response of the thermal lag system. Figure 3a shows three

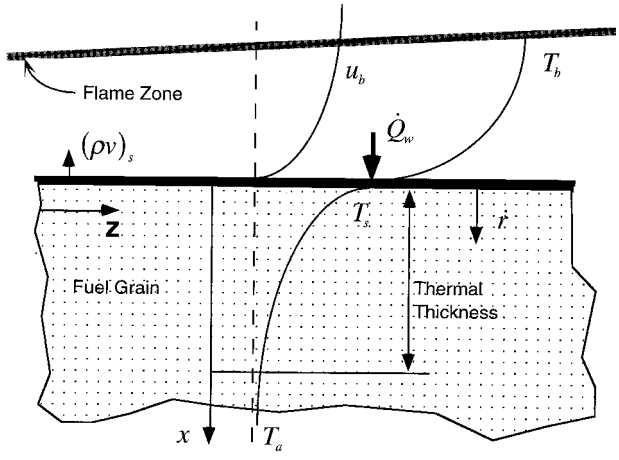

Fig. 1 Schematic of the thermal lag model.

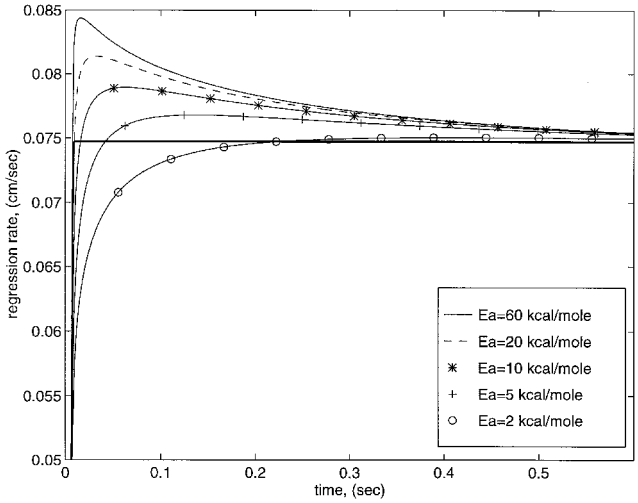

Fig. 2 Effect of activation energy on the regression-rate response for throttling event for a HTPB system with τ_{t1} = 0.4 s. Throttling ratio is 1.5:1.

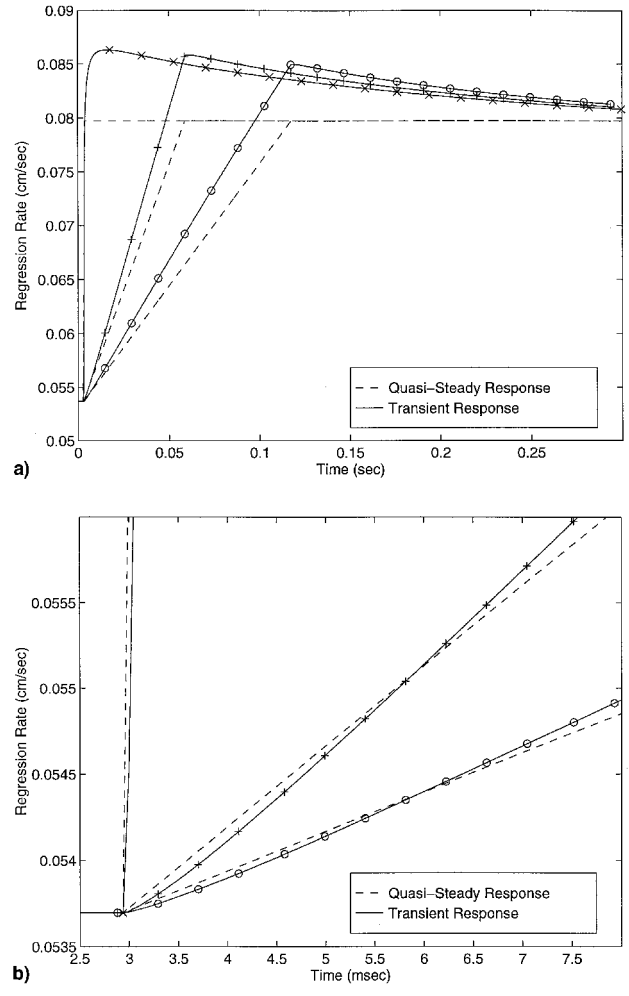

Fig. 3 Effect of throttling rate on the regression-rate response for a polymethylmethacrylate (PMMA) system with τ_{t1} = 0.4 s, E_a = 30 kcal/mole, and a throttling ratio of 1.5:1: a) global and b) initial responses.

numerical simulation results for different throttling rates. The important observation is that, for moderate throttling rates, the transient response anticipates the heat input. This anticipation occurs in the rapid depressurization in solid propellant rockets, leading to the well-known dp/dt extinguishment, when the transient burning rate crosses zero. Similar behavior will be observed in the sinusoidal heat loading case, where the anticipated response is manifested in a phase displacement. However, it can be shown that for all rates there is a small but finite time range (< 10 ms), right after the start of the heat loading, where the response lags the input (see Fig. 3b).

Because of its practical significance, the frequency response of the linearized thermal lag system is investigated to see if the low-frequency instabilities commonly observed in hybrids[6–8] can be explained. We will initially consider the first-order perturbation investigations and later discuss the numerical simulations performed on the full nonlinear system. In the calculations, a sinusoidal surface heat flux perturbation with a specified amplitude and frequency is applied. Because the transfer function of the thermal lag system is already known, the response of the regression rate can easily be calculated with use of the residue theorem.[9] The details of the derivations are presented in the Appendix. Note that we are only interested in the forced response of the system because the natural response decays quite rapidly with respect to the period of low–medium range frequency oscillations.

We first consider the behavior in the two limiting cases of low and high frequency (see Appendix). As expected, at very low frequencies, the regression follows the variations in the wall heat flux in a quasisteady manner with no phase difference [Eq. (A16)]. In the other extreme of very large frequencies, the regression rate lags the wall heat flux with a 45-deg phase angle. The drop of the amplitude of the oscillatory component follows the asymptotic form of $1/\sqrt{\omega}$ at high ω, as indicated in the asymptotic formula [Eq. (A17)].

The response at the intermediate frequencies is quite interesting. As a typical example, we consider a polymethylmethacrylate (PMMA) system (the physical properties used in the calculations are shown in Table 1[5,10]) with a thermal characteristic time of $\tau_{t1} = 0.5$ s. The normalized regression rate amplitudes and phase differences between the regression rate and heat flux are plotted over a range of frequencies in Fig. 4. For convenience, the amplitudes shown in the figure are normalized with respect to the quasisteady response [by Eq. (A16b)]. It is apparent that for relatively small frequencies, $f < 80$ Hz for this system, the regression-rate oscillations are amplified. The amplitude of the regression rate increases from its quasisteady value and takes a maximum value (in the range of 1–10 Hz). For this specific case, the maximum amplitude is ~25% larger than R_1^{qs}. At higher frequencies, the amplitude of the response monotonically decreases with the increasing frequency. At a moderate frequency, in the range of 80 Hz for this system, it crosses the quasisteady amplitude, after which it is attenuated. Eventually, the amplitude response reaches its asymptotic behavior at very high frequencies.

The nature of the phase difference response is also worth noting. In a small range of frequencies close to zero, the regression rate leads the wall heat flux input. Specifically, the phase difference, starting from zero at zero frequency, increases to a maximum phase lead that occurs at a small frequency. Later, the phase difference starts decreasing and it crosses the zero axis (at which the regression rate and the heat flux are in phase one more time). For the frequencies larger

Table 1 Thermophysical properties[5,10] of the propellants used in the calculations

Fuel type	C, cal/g-k	ρ_f, g/cm^3	κ, cm^2/s	L_v, cal/g	T_s[a], K	E_a[b], kcal/mole	E_{E_a}[c]	E_L
PMMA	0.37	1.1	1.1×10^{-3}	231	620	30–40	12.6–14.7	1.94
HTPB	0.57	0.93	1.0×10^{-3}	433	820	12–60	4.7–23.4	1.45

[a]These are the wall temperatures at a specified regression rate, which is 0.05 cm/s for PMMA and 0.075 cm/s for HTPB.
[b]Instead of a single value, we give a range that covers the data in the literature.
[c]Ambient temperature is taken 300 K in the calculations.

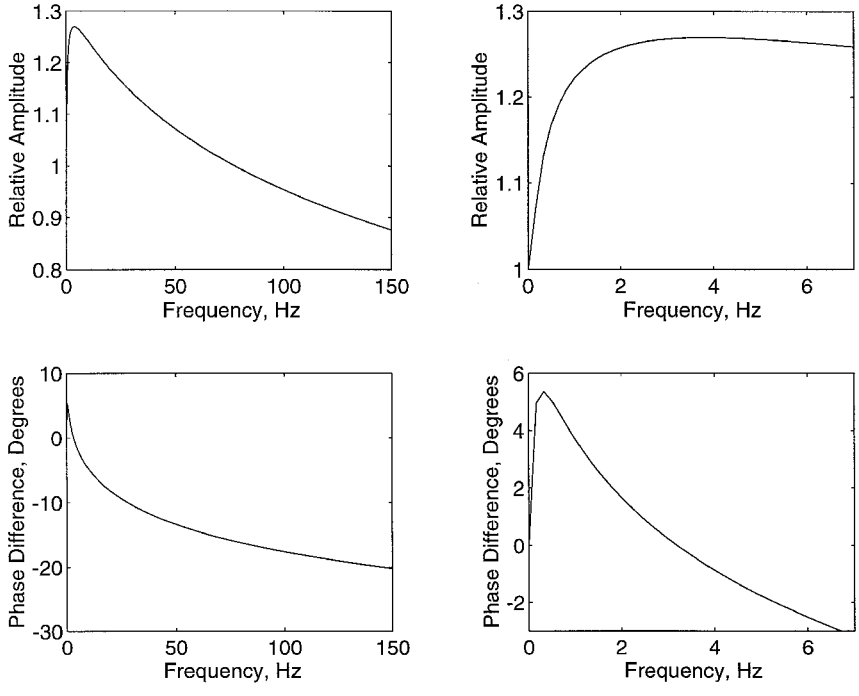

Fig. 4 Frequency response for the thermal lag system. PMMA fuel with E_a = 30 kcal/mole and τ_{t1} = 0.5 s. Right-hand side figures show a close-up to the low-frequency range. The relative amplitude is defined as R_1/R_1^{qs}, where R_1^{qs} is the quasisteady amplitude defined in Eq. (A16b).

than this crossing frequency, the regression always lags the heat flux input that is consistent with observation in Fig. 3b. Eventually, the phase asymptotes to $-\pi/4$ monotonically at very high frequencies, as mentioned previously. In short, for frequencies smaller than this crossing frequency, the regression rate leads the heat flux input, whereas for higher frequencies it lags.

The region of amplitude amplification is much wider than the region of the phase lead in the frequency domain. The amplification of the regression rate is on the order of 20–30% for the practical operating regimes of hybrids. We also note that no resonance behavior is observed for any set of parameters. For that reason it can be stated that the thermal lag system is inherently stable, at least in the linear regime, and that the thermal lags alone cannot generate the low-frequency oscillations observed in hybrids. However, it is shown that, should an instability occur for other reasons, the low-frequency oscillations will be preferentially amplified.

At this point we may inquire whether the classical hybrid can experience an L^* instability as in the solid rocket.[11] It is well known that a solid rocket may experience low-frequency instabilities, if the regression rate leads the pressure oscillations. Because for solids the combustion is most often pressure dependent, the surface heat flux will mainly be a function of the chamber pressure (even during the transients). Thus, it is the phase lead of the regression rate as shown in this paper that generates the L^* instabilities. But the essential ingredient of this type of instability is the explicit dependence of the wall heat flux on the chamber pressure. However, most hybrids do not possess this relationship, because the combustion is mainly diffusion-limited. In short, hybrids do not appear to possess low-frequency instabilities in the L^* theory framework.

The influence of the activation energy on both the amplitude and phase lag is shown in Fig. 5 for an HTPB system operating at a nominal condition corresponding to a characteristic time of $\tau_{t1} = 0.4$ s. The effect of increasing activation energy is to enlarge the amplification and the phase lead regions in the frequency domain. As the activation energy increases, the magnitude of the relative amplification and the value of the maximum phase lead increases. This observation is related to the overshooting phenomenon discussed in the context of throttling. At high activation energies, as described in the preceding section, the surface time scale is small and overshooting is significant. The response can lead and amplify a faster-changing input through the overshooting phenomenon. Thus, the phase lead and amplification domains get larger as the activation energy increases. In the limiting case of infinite activation energy that corresponds to the constant-wall (surface)-temperature model of Ref. 5, the phase lead and relative amplification covers the whole frequency spectrum. Namely, the relative amplification and phase lead increase to their maximum values at a very small frequency, and they stay constant for the whole frequency spectrum. For very small activation energies, the frequency response behaves like the response of a first-order system, with no amplification, which is consistent with no regression-rate overshoot.

It is determined that the effect of the latent heat, L_v, on the frequency response is secondary for the fuels typically used in hybrid applications. The influence of the thermal lag time is to linearly stretch the frequency axis of the response curves such that a system with a smaller thermal lag time will have a broader frequency range of amplification and phase lead.

Some numerical simulations were performed of the sinusoidal heat input case to explore the possible nonlinear effects on the response and to confirm the perturbation analysis results. It may be noted that the results of this perturbation analysis are in good agreement with the numerical simulations, even for relatively high-oscillation amplitudes such as 40% of the mean value.[4] Another important observation that is made from the numerical simulation results is the existence of a small shift of the mean regression rate above the mean quasisteady value. This is consistent with the experimental findings of a dc shift, indicating increased mean regression rates during the oscillatory modes of combustion.

Transient Boundary-Layer Heat Flux

In the previous part of our studies, we treated the surface heat flux as a parameter that can directly be controlled. However, in a hybrid motor, the oxidizer mass flow rate is the primary variable that controls the wall heat flux through other parameters. The actual response of the motor to a change in the oxidizer mass flow is rather complicated during a transient. As the oxidizer mass flow rate of the motor changes, the mass flux at a characteristic point in the port reacts to the change, as does the turbulent boundary layer developed over the fuel surface. In this section we will focus on the modeling of the boundary-layer combustion dynamics and investigate its interactions with the thermal lags in the solid.

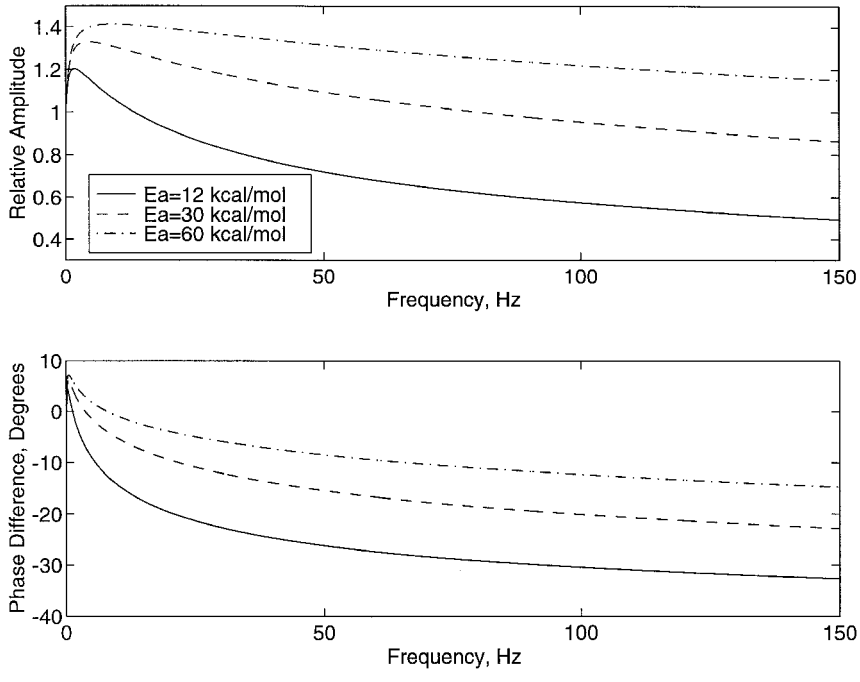

Fig. 5 Effect of activation energy on the frequency response of the thermal lag system. The plot is for a HTPB system with $\tau_{t1} = 0.4$ s. The relative amplitude is defined as R_1/R_1^{qs}, where R_1^{qs} is the quasisteady amplitude defined as Eq. (A16b).

In our preliminary model we assume that the boundary-layer response is quasisteady, namely, the boundary-layer diffusion lag times are small compared with the thermal lag times in the solid. Under the quasisteady assumption, one can use the classical approach[1,2] to calculate the response of the wall heat flux to the changes in mass flux. However, the results of classical hybrid theory cannot be used directly during a transient in the solid, because the convective heat transfer to the wall depends explicitly on the instantaneous regression rate through the blocking generated by the blowing of the gaseous fuel from the surface. In the presence of the thermal lags, the blocking generates a coupling mechanism in the gas phase between the regression rate and the heat flow to the surface.

The convective heat flux from the gas to the fuel surface $\dot{Q}_c$ is given in terms of the heat transfer coefficient C_H at time t as

$$\dot{Q}_c(t) = C_H \rho_b u_b (h_b - h_w) = C_H \rho_b u_b \Delta h \tag{2}$$

where h_b and h_w are enthalpies at the flame and at the wall, respectively. Note that all variables are functions of time.

We will now assume that the classical assumption of Reynolds analogy is still valid during this quasisteady operation mode. This allows us to express the heat transfer coefficient in terms of the skin-friction coefficient as

$$C_H = \tfrac{1}{2} C_f \left(\rho_e u_e^2 \Big/ \rho_b u_b^2 \right) \tag{3}$$

After the elimination of the heat transfer coefficient, we obtain the following expression for the wall heat flux:

$$\dot{Q}_c(t) = \tfrac{1}{2} C_f G (u_e / u_b) \Delta h \tag{4}$$

where G is the total mass flux $\rho_e u_e$.

At this point it is useful to define an aerodynamic blowing parameter (also known as the mass transfer number) as

$$B_a = \frac{(\rho v)_w}{\rho_e u_e C_f / 2} = \frac{\dot{r} \rho_f}{G C_f / 2} \tag{5}$$

The skin-friction coefficient can be written as the skin-friction coefficient for no blowing multiplied by a correction factor, C_f / C_{fo}, for the blocking, which, in general, is a function of the aerodynamic blowing parameter, B_a.

For the blowing correction during transient, we will assume a similar formula to that proposed by Marxman[1]:

$$C_f / C_{fo} = q B_a^{-k} \tag{6}$$

At the steady-state, Eq. (1) becomes $\dot{Q}_c = \dot{r} \rho_f h_v$, which when combined with Eqs. (2) and (3) gives a steady-state value for the thermochemical blowing parameter defined in Eq. (5):

$$B_t = (u_e / u_b)(\Delta h / h_v) \tag{7}$$

Combining Eqs. (4–7) yields the following expression for convective heat flux at the wall:

$$\dot{Q}_c = \tfrac{1}{2} C_{fo} q h_v G B_a^{-k} B_t = \tfrac{1}{2} C_{fo} q G B_a^{-k} (u_e / u_b) \Delta h \tag{8}$$

It is important to observe the distinction between the two forms of the blowing parameter, because during a transient, one must use the general form in Eq. (5), because the regression rate is time dependent and must wait for the temperature gradient at the surface $(\partial T / \partial x)_s$, to adjust, as shown in Eq. (1).

During a transient, the aerodynamic blowing parameter at a given operating condition of a rocket motor cannot be determined by equating it to the thermochemical blowing parameter. However, B_a can be expressed in terms of regression rate and mass flux with the use of Eqs. (5) and (6):

$$B_a = \left(\frac{\dot{r} \rho_f}{q G C_{fo} / 2} \right)^{1/(1-k)} \tag{9}$$

Now, a general form of the heat conduction expression can be found with the substitution of B_a and the commonly used form of the skin-friction coefficient for the turbulent boundary layers,[12] $C_{fo}/2 = 0.03(Gz/\mu)^{-0.2}$ in Eqs. (8) and (9):

$$\dot{Q}_c(t) = \left(\frac{0.03q}{\mu^{-0.2}} \right)^{1/(1-k)} \left[\frac{B_t h_v}{\rho_f^{k/(k-1)}} \right] z^{-0.2/(1-k)} G^{0.8/(1-k)} \dot{r}^{-k/(1-k)} \tag{10}$$

Here, z is the axial distance from the entrance of the port.

Note that the terms in the parentheses in Eq. (10) are functions of the boundary-layer properties and combustion characteristics. Thus, they can be treated approximately as constants after the propellants are selected and the expression for the heat flux reduces to the following form, where A' is a constant for a given propellant combination:

$$\dot{Q}_c(t) = A' z^{-0.2/(1-k)} G^{0.8/(1-k)} \dot{r}^{-k/(1-k)} \tag{11}$$

Up to this point we have developed a formula that relates the wall heat flux at a specified location of the port to the regression rate and mass flux at that location. However, in practice for a specific propellant combination, the coefficient A' is best determined empirically. Very frequently, the available data are based on the average regression rate in terms of the oxidizer mass flux.[3] Let's consider, for simplicity, a propellant combination with the average regression-rate expression for a given grain length $\dot{r} = a G_o^n$. Note that the following analysis can equally be performed for other forms of the regression-rate expressions used for hybrids. Similar to the local formulation, a space-averaged expression can be derived as

$$\dot{Q}_c(t) = \bar{A}' G_o^{n/(1-k)} \dot{r}^{-k/(1-k)} \tag{12}$$

where $\bar{A}' = \rho_f h_v a^{1/(1-k)}$. Here, G_o replaces G and n replaces 0.8 to conform to typical experimental reporting. Note that the heat flux from the gas to the wall depends on the port mass flux and also the regression rate, by virtue of its blocking effect.

To couple the heat-flux expression with the thermal lag formulation, we nondimensionalize with respect to the reference state $(G_o)_{\text{ref}}$, $\dot{Q}_{\text{ref}} (= \dot{r}_{\text{ref}} \rho_f h_v)$ and $\dot{r}_{\text{ref}} [= a (G_o)_{\text{ref}}^n]$, which is selected to be the nominal operating point. In terms of the normalized quantities, $\bar{G}_o = G_o / (G_o)_{\text{ref}}$ and $\bar{\dot{Q}}_c = \dot{Q}_c / \dot{Q}_{\text{ref}}$, the heat flux equation takes the form of Eq. (13):

$$\bar{\dot{Q}}_c(\bar{t}) = E_h \bar{G}_o^{n/(1-k)} R^{-k/(1-k)} \tag{13}$$

Note that $E_h = h_v / C \Delta T = 1 + E_L$, and the rest of the nondimensional variables and parameters used in this expression are defined in the Appendix.

Next, we linearize this equation around the reference point by expanding, as follows:

$$\bar{\dot{Q}}_c(\bar{t}) = 1 + \varepsilon Q_1(\bar{t}) + \mathcal{O}(\varepsilon^2) \tag{14a}$$

$$R(\bar{t}) = 1 + \varepsilon R_1(\bar{t}) + \mathcal{O}(\varepsilon^2) \tag{14b}$$

$$\bar{G}_o(\bar{t}) = 1 + \varepsilon G_1(\bar{t}) + \mathcal{O}(\varepsilon^2) \tag{14c}$$

The first-order terms in ε can be collected to give the linear version of the relation to be used in the first-order perturbation analysis:

$$Q_1(\bar{t}) = E_h \left[\left(\frac{n}{1-k} \right) G_1(\bar{t}) - \left(\frac{k}{1-k} \right) R_1(\bar{t}) \right] \tag{15}$$

Note that in the absence of the blocking effect ($k = 0$ and $q = 1$), the heat flux becomes a function of the oxidizer mass flux alone.

Combustion Boundary-Layer–Thermal Lag Coupling

In the development of the transient hybrid combustion theory, we assumed that the boundary layer responds rapidly to the changes in the mass flux compared with the other transient time scales in the rocket motor such as the gasdynamic lags or the thermal lags. This assumption fails to be valid, particularly for large hybrid motors. To develop a realistic model for the dynamics of the hybrid motor, the boundary-layer lags must be considered. There does not appear to be sufficient information in the literature on the response of the turbulent boundary layers with chemical reactions and blowing, i.e., hybrid rocket combustion scheme, to the changes in the free-flow conditions. Because this complex dynamic phenomenon is extremely difficult to investigate, both theoretically and experimentally, we consider the simpler cases reported in the literature of a standard incompressible turbulent boundary layer with no blowing or chemical reactions. The transient response of various kinds of turbulent flowfields are discussed briefly in Ref. 4. Here, we will restrict our discussion to an important set of transient experiments.[13] The tests were performed by abruptly changing the freestream velocity over a turbulent boundary layer from one value to another (such as throttling) and by measuring the time-average velocity profile and the fluctuations in the velocity components at various axial locations. The researchers concluded that the time required for transition from the initial equilibrium profile to the final equilibrium profile at any axial location was proportional to the time of flight of a fluid particle from the leading edge of the boundary layer to the specific axial location at the speed of the freestream flow. This very important result can be formulated for hybrid boundary layers as

$$\upsilon_{b1} = c'(z/u_e) \tag{16}$$

Here, c' is a constant that needs to be determined empirically. We will call this time required for equilibration, the characteristic response time of the boundary layer, υ_{b1}. It is important to note that the physical nature of the boundary-layer transient time is not related to the propagation of the disturbances with the speed of the port velocity as suggested by Eq. (16). Instead, the delay depends on the diffusion time scale across the boundary layer, which is proportional to the ratio of the local boundary-layer thickness to the diffusion speed, $\upsilon_{b1} \cong \delta/U^*$. The diffusion speed is defined in terms of the shear stress and mean gas density as $U^* = \sqrt{(\upsilon_b/\rho)}$. The boundary-layer delay time, after the substitution of the standard (incompressible) turbulent boundary-layer expressions[12] for the shear stress, $\upsilon_b = 0.0288\rho u_e Re_z^{-0.2}$, and the thickness, $\delta = 0.37zRe_z^{-0.2}$, becomes $\upsilon_{b1} = 2.18Re_z^{-0.1}z/u_e$. Here the local Reynolds number is defined as $Re_z = u_e z\rho/\mu$. Note that the coefficient c' is found to be a weak function of the local Reynolds number. Thus, we assume that c' is constant. For Reynolds numbers corresponding to typical hybrid operation, c' is estimated to be ~ 0.5. In a real hybrid boundary layer with combustion and blowing, c' can be different from this estimation, and for that reason, it is determined empirically.

For the purpose of this paper, it is convenient to consider an average boundary-layer delay and replace the local distance z, with the length of the grain, L. Note that the empirical constant c' accounts for the correction to the inaccurate selection of the length scale, L. However, we recognize that in reality there is a range of boundary-layer delay times that should be considered. Thus, the significant observation here is that an erratic or variable low-frequency instability can result. The exact determination of the average delay time is quite difficult, because the hybrid boundary layers merge at a point that has been estimated to be at an $L/D \approx 5$ (Ref. 14). Note that, after they merge, the diffusion thickness for the oxidizer portion becomes a large fraction of the radius of the port that changes very slowly with the axial distance. However, the diffusion thickness in the fuel side continues to increase because of the increasing distance of the flame from the wall.

In our studies the response of the boundary layer to the changes in the mass flux is accounted for by simply inserting time delays in the heat-flux expressions derived under the assumption of quasisteady response. The implementation of this idea in Eq. (15) yields

$$Q_1(\bar{t}) = E_h\left[\left(\frac{n}{1-k}\right)G_1(\bar{t}-\bar{\upsilon}_{b11}) - \left(\frac{k}{1-k}\right)R_1(\bar{t}-\bar{\upsilon}_{b12})\right] \tag{17}$$

where $\bar{\upsilon}_{b11} = \upsilon_{b11}/\upsilon_1$ and $\bar{\upsilon}_{b12} = \upsilon_{b12}/\upsilon_1$.

Here, υ_{b11} and υ_{b12} are the time delays experienced by the wall heat flux (Q_c) to the changes in the oxidizer mass flux and the regression rate, respectively. The scaling of the time delays υ_{b11} and υ_{b12} obey the general scaling law given by Eq. (16). However, the c' coefficients for υ_{b11} and υ_{b12} are expected to be different because each of these delays represents a different adjustment mechanism for the boundary layer.

Now, with the use of this relation, the thermal lags in the solid can be coupled to the combustion transients in the boundary layer. This coupling will yield a transfer function between the oxidizer mass flux (input) and the regression rate (output).

The derivation of the transfer function is very similar to the derivation performed for the pure thermal lag case. The only difference is the energy balance boundary condition at the surface that must be modified. Substitution of Eq. (17) in the surface boundary condition of the linearized thermal lag problem [Eq. (A11)] yields the correct boundary condition for the coupled problem:

$$\left(\frac{\partial T_1}{\partial x}\right)_{x=0} - E_L R_1(\bar{t}) - \sigma_1 R_1(\bar{t}-\bar{\upsilon}_{b12}) = -\sigma_2 G_1(\bar{t}-\bar{\upsilon}_{b11}) \tag{18}$$

Two new constants are introduced for convenience:

$$\sigma_1 = E_h[k/(1-k)], \qquad \sigma_2 = E_h[n/(1-k)] \tag{19}$$

With this new boundary condition the linearized thermal lag problem can be solved in a similar way to the case with no delays, with the use of the Laplace transformation technique. The transfer function between the regression rate $[R_{1L}(s)]$ and the mass flux $[I(s)]$ can be obtained as

$$\frac{R_{1L}(s)}{I(s)} = \frac{2E_{E_a}\sigma_2 e^{-\bar{\upsilon}_{b11}s}s}{\left(1+\sqrt{1+4s}\right)\left(s+E_{E_a}\right) - 2E_{E_a} + 2E_{E_a}s\left(E_L + \sigma_1 e^{-\bar{\upsilon}_{b12}s}\right)} \tag{20}$$

This transfer function, which represents the combustion phenomenon, includes the dynamics of the thermal processes in the solid and approximates the combustion dynamics in the turbulent boundary layer of the rocket motor.

Results and Discussion

We are now in a position to investigate the behavior of the regression rate caused by the changes in the oxidizer mass flux with the use of Eq. (20). The dynamic characteristics of the hybrid combustion system can be deduced (at least in theory) from the properties of this transfer function. This transfer function includes the latent and activation energy parameters E_L and E_{E_a}, the B and G exponents (k and n), and the delay times of the boundary layer. (In the calculations, the $k = 0.68$ value suggested by Ref. 3 and $E_a = 15$ kcal/mole for HTPB fuel are used.) In that respect, the dynamic behavior of the combustion will depend on these parameters, and in this section we will investigate the impact of those on the system dynamics.

One of the most important properties of the system of practical interest is the inherent stability of the hybrid combustion scheme. As discussed earlier in this paper, low-frequency instabilities are widely observed in actual motors of various sizes. In general, for dynamic systems with analytic transfer functions, the stability feature of the system can be directly examined by the open loop transfer function with use of the Nyquist stability criterion.[15] For systems with time delays, a very clever technique was developed that is a variation of the standard Nyquist criterion.[16] However, our system transfer function is significantly more complicated, because it is not an analytic

function in the complex s domain.[9] This is a characteristic of the diffusive systems that yield a square root term, which automatically introduces a branch point in their Laplace transforms. Because the transfer function is not an analytic function of the Laplace transform variable s, the Cauchy integral theorem does not hold and the standard Nyquist stability criterion or the Satche criterion derived from it cannot be applied directly. However, it is shown[4] that we can still state that the system will be unstable if at least one of poles of the transfer function has a positive real component for the system to be unstable. The poles can be determined by finding the roots of the characteristic equation (the denominator of the transfer function). The imaginary portion of the root is the oscillation frequency of the system, whereas the real part is the amplification rate of the corresponding frequency.[15] In other words, the unstable oscillation frequency of the system will be the imaginary part of a pole with a positive real component.

We first observe that the delay between the heat flux and the oxidizer mass flux, τ_{b11}, does not affect the stability characteristics of the boundary-layer–thermal lag (BL–TL) coupled system, because its appearance is limited to the numerator of the transfer function given by Eq. (20). We will start with the trivial case with no boundary-layer delay between the wall heat flux and oxidizer mass flux. A careful analysis shows that, similar to the pure thermal lags case, the system with no boundary-layer delays does not have any poles. This can be seen from Fig. 6a, which is a plot of the transfer function for $\tau_{b12} = 0$ over the complex plane. It is clearly a smooth function in the domain of interest. A systematic search for a pole is performed for various combinations of the parameters and no poles are found. We conclude that a system without boundary-layer delays is always stable in this mode.

On the contrary, a system with delay between the regression rate and the heat flux ($\tau_{b12} \neq 0$) showed interesting behavior. As can be seen from Fig. 6b, which is also a plot of the transfer function

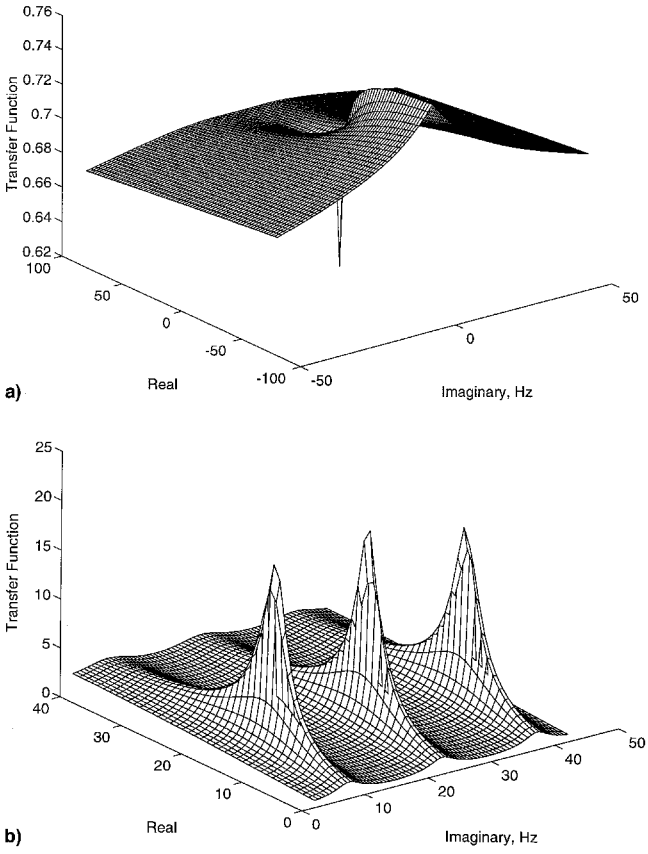

Fig. 6 a) Plot of the transfer function of the BL–TL coupled system with no delays ($\tau_{b11} = \tau_{b12} = 0$). b) The unstable poles of the BL–TL coupled system in the s plane for $\tau_{b11} = 0$, $\tau_{b12} = 66.7$ ms, and $\tau_{t1} = 118.6$ ms. These plots are for a HTPB system with $E_a = 15$ kcal/mole.

over the s domain, the system has several poles in the positive real part of the s plane. These roots indicate that the system will possess an unstable time-domain response. These calculations were made with a time delay (τ_{b12}) of 66.7 ms that corresponds to a motor with an average gas velocity of 45 m/s, a length of 6 m, and a c' of 0.5. Note that there is a series of unstable frequencies, all with the same amplification rate, and the smallest of those frequencies corresponds to the range of low-frequency instabilities observed in practice for that motor size. We suggest that the higher-frequency instabilities, although appearing at the same amplification rate as the lowest frequency because of the linear theory, will possibly be stabilized by the nonlinear effects and the energy dissipation processes. It is also determined that the thermal lag time does not affect the value of the fundamental oscillation frequency of the system.

To explore the compatibility of the results of this linear model with the observations, we will perform two parametric studies and compare those with the test results from the actual motor runs. The first one of those is for the various-sized American Rocket Company (AMROC) motors,[17] which operated at various L^* levels. Because the information on the AMROC motors that can be found in the literature is limited to L^*, c^*, and a motor's O/F ratio, it is desirable to express the boundary-layer delay time [Eq. (16)] in terms of those variables. The average velocity in the port can be approximated as

$$u_{\text{av}} = \frac{G_t[(1+2O/F)/(1+O/F)]R_gT_{\text{av}}}{2P_c}$$

where R_gT_{av} is an average value in the port. Substituting this expression in the delay formula and using the relations for the total mass flow rate $\dot{m}_t = G_tA_p$ and port volume $V_p = LA_p$, yields

$$\tau_{b1} = c'\frac{2V_pP_c}{\dot{m}_t[(1+2O/F)/(1+O/F)]R_gT_{\text{av}}}$$

With the use of the total mass flow relation, $\dot{m}_t = PA_n/c^*_{\text{exp}}$, and the definition $L^* = V_m/A_n$, the delay equation can be written as

$$\tau_{b1} = 2c'\frac{V_p}{V_m}\frac{[(1+O/F)/(1+2O/F)]}{R_gT_{\text{av}}}L^*c^*_{\text{exp}} \qquad (21)$$

Here, V_p/V_m is the ratio of the port volume to the motor free volume, which is estimated to be ~0.8 for the AMROC DM-01 motor.[17] We assume that all AMROC motors possess the same average gas constant temperature product, R_gT_{av}, and volume ratio, V_p/V_m. Various properties of the AMROC motors[6,17] are listed in Table 2. After noting that all motors operate at very similar O/F ratios and c^*_{exp} values, it can be noted that in the series of tests the boundary-layer characteristic delay time is proportional to L^*.

We estimated the fundamental oscillation frequencies predicted by the linear theory for various boundary-layer delays. The result is shown in Fig. 7, which is a plot of the calculated unstable oscillation frequency vs the boundary-layer delay of the motor. The AMROC motor data are also included in this figure. A c' value of 0.79 is selected to provide a best fit between the linear theory predictions and the observed frequencies of the AMROC motor tests. As indicated in the figure for this selected delay coefficient, the linear theory estimates the AMROC motor instability frequencies with good accuracy.

The plot clearly shows the inverse relation between the boundary-layer delay time and the fundamental oscillation frequency. Moreover, when Fig. 7 is plotted in the log–log scale, the oscillation

Table 2 Summary of parameters used in the frequency estimations for AMROC motors

AMROC motor (thrust)	O/F	c^*_{theo}, m/s	c^*_{exp}, m/s	L^*, m	f, Hz
S motor (10 k)	1.45	1702	1634	14.5	11
Half-scale (33 k)	1.45	1702	1634	33.2–36.3	4.8
H-500 (75 k)	1.45	1702	1634	45.0–59.4	4.0
DM-01 (250 k)	1.55	1737	1668	55.0	2–3.5

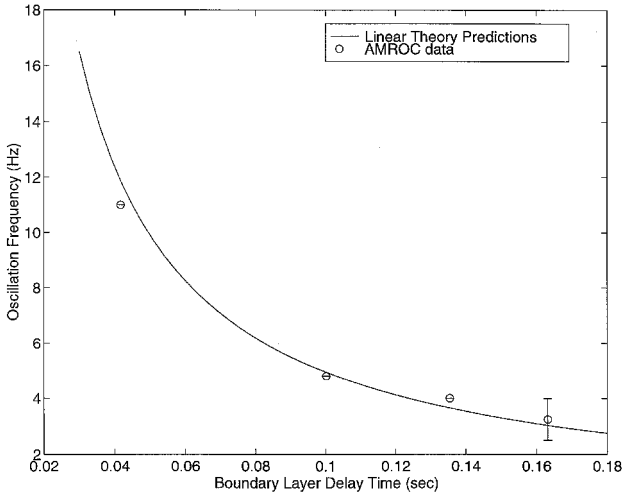

Fig. 7 Effect of motor size on the oscillation frequency. Comparison of the BL–TL coupled theory with the AMROC motors instability data.

frequency shows a linear variation with the boundary-layer delay time. This suggests that the frequency is inversely proportional to the delay time or

$$f = \text{const}/\,\upsilon_{b1} \tag{22}$$

where the constant has a value of 0.50 for this specific case. For AMROC motors that operate at approximately the same O/F levels, the frequency becomes inversely proportional to L^*. This relation has been previously observed.[18]

A different test of the model can be performed by comparing the predictions with actual experimental results for motors with the same port length, but running at different operating points; i.e., chamber pressure, oxidizer mass flux, port diameter. To treat this case, the port velocity can be replaced by an average value $(G_o + G_t)/2\rho_{av}$ with ρ_{av} given by the gas law $P_c = \rho_{av} R_g T_{av}$ to yield for the boundary-layer lag:

$$\upsilon_{b1} = c' \frac{2LP_c}{(G_o + G_t) R_g T_{av}} \tag{23}$$

Eq. (23) reveals that delay increases with increasing chamber pressure and port length, and that delay decreases with increasing mass flux in the port. Combining Eqs. (22) and (23) indicates that an increase in the chamber pressure or a decrease in the port mass flux act to decrease the oscillation frequency of this type of BL–TL coupled system.

The predictions are tested in Ref. 4, which mainly used the 11-in. gaseous oxygen hybrid motor tests, which were performed with HTPB/Escorez fuel grains.[7,8] It was found that the estimated oscillation frequencies were in reasonable agreement with the observed ones. The delay constant in the calculations is determined to be 0.63 by fitting the experimental data to the theory predictions. It is significant that the boundary-layer delay coefficients obtained for the AMROC motors and also for the 11-in. motors are reasonably close to each other, and also to the theoretically predicted value of 0.5 for an incompressible turbulent boundary layer with no blowing.

The impact of the parameters other than the boundary-layer delay time (such as the fuel properties including the activation energy or the mass flux and blowing exponents) on the oscillation frequency is determined to be small. It is also observed that decreasing activation energy (E_a) and decreasing blowing exponent (k) decreases the amplification rate (real component of the poles) of the oscillatory modes. The effect of the other parameters such as the mass flux exponent and the latent heat of gasification on the amplification rate is negligible. In the extreme case of a no blocking effect ($k = 0$), this model shows that the system does not possess an oscillatory component in its natural response (either stable or unstable). Thus, for highly radiating combustion gases, where the effective k values are diminished, we might expect that the tendency for instability from this mechanism would be decreased. Within the reasonable range of variations in the activation energy and the blowing exponent, the changes in the amplification rate are small. This may serve as an explanation on why the low-frequency oscillations are encountered for a wide range of motors.

Conclusions

The thermal lag system dynamics that determines the regression-rate response during a transient heat loading is represented with two time scales. One is a short lag near the surface related to the activation energy, and the other is the longer well-known thermal lag as a result of conductivity. These delays cause an overshoot of the regression rate during throttling, the degree of which depends on the percent throttle, throttling rate, and activation energy. The activation energy determines the surface temperature excursion during the throttle, and therefore, the surface time lag. When applied to an oscillating heat flux, an amplification of the regression rate is observed for low frequencies, which can aggravate an existing instability, but not cause it.

One mechanism explored, which can create an instability, is the coupling of the regression rate with the wall heat flux through the boundary-layer processes and the thermal diffusion in the solid. The linear theory developed shows the frequencies and exponential amplification rates based on the boundary-layer adjustment lag and other relevant parameters of the problem. The most significant result of the treatment is prediction of the low-frequency oscillations, which is in good agreement with experimental observations and its explanation of the erratic nature of the instability. The amplitude of the pressure oscillations in a hybrid motor chamber during the instability is bounded, and it has the character of a limit cycle process. The linear theory, of course, can only yield an unlimited increase of the oscillation amplitude through exponential growth in time. The energy dissipation and nonlinear processes in a motor must be considered to determine the limiting amplitudes in the instabilities. A more complete hybrid stability theory requires a good understanding of those nonlinear effects and should include the interaction with the gasdynamics in the chamber involving pre- and postcombustion chambers.

Appendix: Thermal Lag Formulation

The model for the thermal lags in the solid is shown in Fig. 1. The heat diffusion equation expressed in the coordinate system moving with the regressing surface is

$$\frac{\partial T}{\partial t} = \kappa \frac{\partial^2 T}{\partial x^2} + \dot{r}(t) \frac{\partial T}{\partial x} \tag{A1}$$

The two required boundary conditions are

$$x \to \infty, \qquad T = T_a, \qquad \frac{\partial T}{\partial x} = 0 \tag{A2}$$

$$x = 0, \qquad \dot{Q}_w(t) = \rho_f \dot{r}(t) L_v - \lambda \left(\frac{\partial T}{\partial x} \right)_s \tag{A3}$$

Note that these boundary conditions, with the appropriate form of the wall heat transfer, are common for every transient event. However, the initial condition that is the temperature distribution at the start of the event is case dependent.

A constitutive relation modeling the surface processes is required to close the set of equations representing the mathematical formulation of thermal lag theory. The gasification and pyrolysis reactions at the surface are both generated by an exponential of the Arrhenius type. For chemical reactions, the exponential constant is an activation energy, whereas in vaporization it is the latent heat. To describe this behavior, we assign an average effective activation energy, resulting in

$$\dot{r} = A \exp(E_a / R_g T_s) \tag{A4}$$

In the thermal lag model, we represent various transient events with the suitable selection of the initial conditions and the wall heat transfer variations. Our goal is to obtain the response of the regression rate during those simulated events. This requires the solution of the coupled Eqs. (A1–A4), resulting in a nonlinear moving boundary problem, and an exact closed-form solution is not available.

The variables can be normalized with respect to a reference state that can be defined by the reference set $[(G_o)_{\text{ref}}, (\dot{Q}_s)_{\text{ref}}, \dot{r}_{\text{ref}}, (T_s)_{\text{ref}}, \mathcal{U}_{\text{ref}}, \delta_{\text{ref}}]$. Note that the reference time and distance are related to the reference regression rate as $\mathcal{U}_{\text{ref}} = \kappa/\dot{r}_{\text{ref}}^2$ and $\delta_{\text{ref}} = \kappa/\dot{r}_{\text{ref}}$. Note that if the reference point is selected to be the nominal operating condition, the reference time scale becomes identical to the characteristic time for thermal lags in solid, $\mathcal{U}_{\text{l}} = \mathcal{U}_{\text{ref}}$ and $\bar{t} = t/\mathcal{U}_{\text{ref}}$.

It is convenient to normalize the system equations with respect to the reference state. This operation yields the nondimensional form of the equations:

$$\frac{\partial \bar{T}}{\partial \bar{t}} = \frac{\partial^2 \bar{T}}{\partial \bar{x}^2} + R(\bar{t})\frac{\partial \bar{T}}{\partial \bar{x}} \tag{A5}$$

Boundary conditions:

$$\bar{x} \to \infty\text{: } \bar{T} = 0, \qquad \frac{\partial \bar{T}}{\partial \bar{x}} = 0 \tag{A6}$$

$$\bar{x} = 0\text{: } \left(\frac{\partial \bar{T}}{\partial \bar{x}}\right)_s = E_L A \exp\left(-\frac{a'}{\bar{T}_s + b'}\right) - \bar{Q}(\bar{t}) \tag{A7}$$

where $a' = E_a/R_g\Delta T$ and $b' = T_a/\Delta T$.

Regression rate expression:

$$R = \bar{A}\exp\{-[a'/(\bar{T}_s + b')]\} \tag{A8}$$

The following nondimensional variables and parameters of the problem have been introduced:

$$R = \dot{r}/\dot{r}_{\text{ref}}, \qquad \bar{t} = t/\mathcal{U}_{\text{ref}}, \qquad \bar{x} = x/\delta_{\text{ref}}$$

$$\bar{T} = (T - T_a)/\Delta T, \qquad \Delta T = (T_s)_{\text{ref}} - T_a$$

$$\bar{Q} = \dot{Q}_w/\dot{r}_{\text{ref}}\rho_f C\Delta T, \qquad E_L = L_v/C\Delta T$$

$$E_h = h_v/C\Delta T, \qquad \bar{A} = \exp[E_a/R_g(T_s)_{\text{ref}}]$$

Next, we will perform a regular perturbation investigation on the nondimensional system. We first apply a small perturbation heat flux around the reference point, which is selected as the nominal operating condition of the motor [Eq. (14a)]. We assume a regular perturbation on the regression rate [Eq. (14b)] and the temperature:

$$\bar{T}(\bar{x}, \bar{t}) = \bar{T}_{\text{ref}}(\bar{x}) + \varepsilon \cdot \bar{T}_1(\bar{x}, \bar{t}) + \mathcal{O}(\varepsilon^2)$$

Because the reference point is the nominal operating condition, the reference temperature distribution is identical to the steady-state distribution:

$$\bar{T}_{\text{ref}}(\bar{x}) = \exp(-\bar{x}) \tag{A9}$$

Upon substituting the perturbation expressions and the reference state information in the normalized system equations, and collecting the order of ε terms together, we obtain the following linear initial-boundary problem for the first-order perturbation quantities:

$$\frac{\partial \bar{T}_1}{\partial \bar{t}} = \frac{\partial^2 \bar{T}_1}{\partial \bar{x}^2} + \frac{\partial \bar{T}_1}{\partial \bar{x}} - E_{E_a}\bar{T}_1\Big|_{\bar{x}=0}\exp(-\bar{x}) \tag{A10}$$

Boundary conditions:

$$\left.\frac{\partial \bar{T}_1}{\partial \bar{x}}\right|_{\bar{x}=0} - E_L E_{E_a}\bar{T}_1\Big|_{\bar{x}=0} = -Q_1(\bar{t}), \qquad \bar{T}_1|_{\bar{x}\to\infty} = 0 \tag{A11}$$

Initial condition:

$$\bar{T}_1 = 0 \tag{A12}$$

Regression rate equation:

$$R_1 = E_{E_a}\left.\frac{\partial \bar{T}_1}{\partial \bar{x}}\right|_{\bar{x}=0} \tag{A13}$$

Here, E_{E_a} is another energy parameter that is proportional to the activation energy:

$$E_{E_a} = \frac{E_a \Delta T}{R_g (T_s)_{\text{ref}}^2} \tag{A14}$$

The linear initial boundary-value problem defined for the first-order perturbation quantities is solved with use of the Laplace transformation technique. The transfer function between the regression rate perturbation and the applied heat flux perturbation, which is a result of practical importance, is given as

$$\frac{R_L(s)}{Q_L(s)} = \frac{2E_{E_a}s}{\left(1 + \sqrt{4s+1}\right)\left(s + E_{E_a}\right) - 2E_{E_a} + 2E_L E_{E_a} s} \tag{A15}$$

$R_L(s)$ and $Q_L(s)$ are the Laplace transforms of the regression rate perturbation and the wall heat flux perturbation, respectively. We now apply a sinusoidal heat input, $Q_1(\bar{t}) = \sin(\bar{\omega}\bar{t})$, which has the Laplace transformation $Q_L(s) = \bar{\omega}/(s^2 + \bar{\omega}^2)$. Note that $\bar{\omega}$ is the nondimensional frequency. The corresponding dimensional angular frequency is $\omega = \bar{\omega}/\mathcal{U}_{\text{l}}$, where $\mathcal{U}_{\text{l}}$ is the thermal lag time corresponding to the nominal operating point.

Coupling $Q_L(s)$ with the transfer function yields the response function of the regression rate, $R_L(s)$, in the s domain. Inverse transformation back to the time domain can be achieved with the use of the residue theorem. In the analysis, we are only interested in the forced response, because the influence of the natural response is expected to be confined in a relatively small time period for practically significant applications. This fact is confirmed by the numerical simulations.

We consider the two limiting behaviors for which the explicit expressions can be relatively easily obtained. The first limit is the low-frequency case ($\bar{\omega} \to 0$), in which the response simplifies to

$$R_1(\bar{t}) = R_1^{\text{qs}}\sin(\bar{\omega}\bar{t}) \tag{A16a}$$

where the amplitude can be written as

$$R_1^{\text{qs}} = \frac{E_{E_a}}{E_L E_{E_a} + E_{E_a} + 1} \tag{A16b}$$

This formula shows that the regression rate follows the heat input in a quasisteady manner as expected. The other limit behavior is the high-frequency one where the response becomes

$$R_1(\bar{t}) = \left(E_{E_a}\Big/\sqrt{\bar{\omega}}\right)\sin[\bar{\omega}\bar{t} - (\pi/4)] \tag{A17}$$

As indicated by this formula, at very high frequencies, the amplitude decreases as $1/\sqrt{\bar{\omega}}$ and the phase difference approaches its asymptotic value $-\pi/4$.

Acknowledgments

This work was performed under partial support from the Department of Aeronautics and Astronautics, Stanford University, and UTC Chemical Systems Division.

References

[1] Marxman, G. A., "Combustion in the Turbulent Boundary Layer on a Vaporizing Surface," *Proceedings of the 10th Symposium on Combustion*, The Combustion Inst., Pittsburgh, PA, 1965, pp. 1337–1349.

[2] Marxman, G. A., Wooldridge, E., and Muzzy, J., *Fundamentals of Hybrid Boundary Layer Combustion*, Vol. 15, Progress in Astronautics and Aeronautics, AIAA, New York, 1964, pp. 485–522.

[3] Altman, D., and Humble, R., "Hybrid Rocket Propulsion Systems," *Space Propulsion Analysis and Design*, McGraw–Hill, New York, 1995, pp. 365–441.

[4] Karabeyoglu, M. A., "Transient Combustion in Hybrid Rockets," Ph.D.

Dissertation, Dept. of Aeronautics and Astronautics, Stanford Univ., Stanford, CA, Aug. 1998.

[5]Karabeyoglu, M. A., Altman, D., and Bershader, D., "Transient Combustion in Hybrid Rockets," AIAA Paper 95-2691, July 1995.

[6]Guthrie, D. M., and Wolf, R. S., "Non-Acoustic Combustion Instability in Hybrid Rocket Motors," AMROC Co., N 91-24250, Camarillo, CA, July 1991.

[7]Boardman, T. A., Brinton, D. H., Carpenter, R. L., and Zolods, T. F., "An Experimental Investigation of Pressure Oscillations and Their Suppression in Subscale Hybrid Rocket Motors," AIAA Paper 95-2689, July 1995.

[8]Boardman, T. A., Carpenter, R. L., and Claflin, S. L., "A Comparative Study of the Effects of Liquid-Versus Gaseous-Oxygen Injection on Combustion Stability in 11-Inch-Diameter Hybrid Motors," AIAA Paper 97-2936, July 1997.

[9]Zodor, G., *Laplace Transformations in Engineering*, Akademiai Kiado, Budapest, 1965.

[10]Esker, D. R., and Brewster, M. Q., "Laser Pyrolysis of Hydroxyl-Terminated Polybutadiene," *Journal of Propulsion and Power*, Vol. 12, No. 2, 1996, pp. 296–301.

[11]Beckstead, M. W., and Price, E. W., "Nonacoustic Combustion Instability," *AIAA Journal*, Vol. 5, No. 11, 1967, pp. 1989–1996.

[12]Schlichting, H., *Boundary Layer Theory*, McGraw–Hill, New York, 1955, Chap. 21.

[13]Parikh, P. G., Jayaraman, R., Reynolds, W. C., and Carr L. W., "Transient Response of a Turbulent Boundary Layer," FED-Vol. 12, American Society of Mechanical Engineers, New York, 1984, pp. 31–40.

[14]Wooldrige, E., and Muzzy, J., "Internal Ballistic Considerations in Hybrid Rocket Design," AIAA Paper 66-628, June 1966.

[15]Cannon, R. H., *Dynamics of Physical Systems*, McGraw–Hill, New York, 1967, Chap. 17.

[16]Crocco, L., and Cheng, S. I., "Theory of Combustion Instability in Liquid Propellant Rocket Motors," AGARD 8, Butterworths, London, 1956, pp. 163–167.

[17]McFarlane, J. S., Kniffen, R. J., and Lichatowich, L., "Design and Testing of AMROC's 250,000 lbf Thrust Hybrid Motor," AIAA Paper 93-2551, June 1993.

[18]Jenkins, R. M., and Cook, J. R., "A Preliminary Analysis of Low Frequency Pressure Oscillations in Hybrid Rocket Motors," AIAA Paper 95-2690, July 1995.